



Gene expression changes are associated with severe bone loss and deficient fracture callus formation in rats with complete spinal cord injury

Mariana M. Butezloff¹ · José B. Volpon¹ · João P. B. Ximenez² · Kelly Astolpho¹ · Vitor M. Correlo³ · Rui L. Reis³ · Raquel B. Silva⁴ · Ariane Zamarioli¹

Received: 17 April 2019 / Revised: 21 October 2019 / Accepted: 23 October 2019 / Published online: 7 November 2019

© The Author(s), under exclusive licence to International Spinal Cord Society 2019

Abstract

Study design Animal study.

Objectives To investigate the effects of SCI on bone quality and callus formation.

Setting University and hospital-based research center, Ribeirão Preto Medical School, Brazil.

Methods Rats sustaining a complete SCI for 10 days received a fracture at the femoral diaphysis and were followed-up for 14 days. Bone callus and contralateral nonfractured tibia were assessed by DXA, μ CT, ELISA, histomorphometry, immunohistochemistry, biomechanical test, and gene expression.

Results SCI downregulated osteoblastic-related gene expression in the nonfractured tibias, associated with a twofold increase in osteoclasts and overexpression of RANK/RANKL, which resulted in lower bone mass, impaired micro-architecture, and weaker bones. On day 14 postfracture, we revealed early and increased trabecular formation in the callus of SCI rats, despite a marked 75% decrease in OPG-positive cells, and 41% decrease in density. Furthermore, these calluses showed higher porosity and thinner newly formed trabeculae, leading to lower strength and angle failure.

Conclusions SCI-induced bone loss resulted from increased bone resorption and decreased bone formation. We also evidenced accelerated bone healing in the SCI rats, which may be attributed to the predominant intramembranous ossification. However, the newly formed bone was thinner, less dense, and more porous than those in the non-SCI rats. As a result, these calluses are weaker and tolerate lesser torsion deformation than the controls, which may result in recurrent fractures and characterizes a remarkable feature that may severely impair life quality.

Supplementary information The online version of this article (<https://doi.org/10.1038/s41393-019-0377-y>) contains supplementary material, which is available to authorized users.

✉ Ariane Zamarioli
arianezamarioli@usp.br

- ¹ School of Medicine of Ribeirão Preto, University of São Paulo, São Paulo, Brazil
- ² School of Pharmaceutical Sciences of Ribeirão Preto, University of São Paulo, São Paulo, Brazil
- ³ 3B's Research Group – Biomaterials, Biodegradables and Biomimetics, Headquarters of the European Institute of Excellence on Tissue Engineering and Regenerative Medicine, University of Minho, Braga, Portugal
- ⁴ School of Dentistry of Ribeirão Preto, University of São Paulo, São Paulo, Brazil

Introduction

Spinal cord injury (SCI) is well known to induce severe osteoporosis in sublesional bones, which leads to an increased risk of low-impact fractures [1–4]. As a consequence, nearly 70% of people with SCI will fracture their bones at some point in their life after injury [3]. Furthermore, hospitalization is longer for these patients, and the incidence of complications is higher [1]. Considering that ~285,000 individuals are living with SCI in the US, the social and medical impact of SCI-induced-bone loss is of great importance [5]. The annual incidence of fractures in individuals with SCI ranges from 2 to 6% but may increase up to 25% in severely affected patients [6].

To maintain the integrity and capability of bone strength and elasticity, a balanced coupling should be preserved between bone formation and resorption. In our previous study, we reported an intense and rapid increase in

osteoclastic activity in rats with paraplegia [7], which lead to significant bone loss and lower capacity to absorb energy before fracturing [2]. The mechanism of bone healing and the quality of the healed bone following SCI are poorly understood. The topic remains very controversial as previous results have shown that callus formation in SCI individuals can be either delayed [6, 8, 9] or accelerated [4, 10, 11]. Experimental studies have been conducted to better understand bone healing in SCI animals. Nevertheless, the conclusions remain controversial, with some authors evidencing early and accelerated fracture healing [12, 13], while others showed delayed healing with poor callus formation [14, 15].

Therefore, this study was conducted to determine the impact of SCI on gene expression, levels of bone markers in serum, bone density, bone microarchitecture, bone cells activity, and the bone strength at both the nonfractured proximal tibial metaphysis and the fractured femoral diaphysis. We hypothesize that SCI severely disrupts the microenvironment of nonfractured bones and impairs bone callus formation and quality.

Methods

The Institutional Animal Care and Use Committee previously approved all animal care and experiments carried out in this study (protocol 199/2015).

Seven-week-old male Wistar rats weighing 200 g (± 10 g) were obtained from the central animal facility of our institution and housed in individual cages with environmental enrichment in a room with controlled conditions of humidity (55–60%), temperature (23 ± 1 °C), and an artificial light/dark cycle of 12 h. The experimental procedures were started after a three-day-interval to allow adaptation to the laboratory environment.

Thirty-six rats were randomly divided into two groups ($n = 18$ per group): (1) Sham + fracture: nonparaplegic rats sustaining a femur fracture; (2) SCI + fracture: SCI rats with femur fracture. Additional sixteen rats were used to replace the losses in the SCI group throughout the study. All rats were inspected daily and weighed to monitor their general health. All experimental procedures (surgeries and euthanasia) were carried out at the same time (early in the morning), in the same surgical room and laboratory environment, including personnel, to maintain the same conditions. Also, in order to reduce external interferences into the results, both groups were developed at the same time.

SCI, postoperative care, and femoral fracture

All rats were anesthetized by intramuscular (IM) injection of ketamine (60 mg/kg, IM) and xylazine (7.5 mg/kg, IM).

Complete SCI was achieved by surgical transection of the cord at the T10 vertebral level, as previously described [7]. The sham-operated animals underwent a laminectomy, with cord exposure but without transection. The daily postoperative care consisted of a general health assessment (including signs of stress), skin examination, neurological functional assessment to confirm immediate and persistent sublesional paralysis, and bladder expression twice a day. All rats were administered buprenorphine (0.03 mg/kg) intramuscularly twice daily for five days for postoperative pain, and 10 mL of Lactated Ringer's solution was injected subcutaneously once a day for five days to prevent dehydration. The groups were followed postoperatively for 24 days.

After ten days of SCI (or sham surgery) the animals were anesthetized and a femoral fracture was produced in the right diaphysis, as previously described [16]. Immediately, under surgical conditions, an incision was made at the lateral side of the tibia, and the fracture was approached, inspected and intramedullary fixed by a 1.0 mm thick surgical Kirschner wire. An X-ray was taken to check for the fracture and fixation adequacy. Any fracture not located at the bone midshaft, or excessively fragmented (three or more fragments of bone), was excluded. Rats were allowed to recover postoperatively. Buprenorphine (0.03 mg/kg) was used for analgesia and injected intramuscularly for five days. The operated animals were examined daily to check for the general health, spontaneous activity, mobility, weight bearing, skin integrity, wound appearance, swelling, and range of motion of the knee and hip. Another X-ray was taken just after the euthanasia.

Euthanasia and sample harvesting

Fourteen days postfracture, rats were sacrificed with excessive anesthetic dosage, and samples were collected for further blinded analysis. Nonfractured contralateral tibias were used to assess bone quality, and the fractured femurs were used to analyze bone healing.

RNA isolation and real-time PCR assessment

Total RNA was extracted from both the fracture callus and the nonfractured tibias ($n = 6$ /bone/group) using an SV Total RNA Isolation System (Promega, Madison, Wisconsin, USA). Complementary DNA (cDNA) synthesis was performed with 1 μ g RNA using High Capacity cDNA Reverse Transcription Kit (Applied Biosystems, Foster City, CA, USA). TaqMan® gene expression assays (Applied Biosystems) were used for quantifying collagen type 1, alpha 2 (*Colla1*), runt-related transcription factor 2 (*Runx2*), and osterix (*Osx*) expression by quantitative PCR on a StepOnePlus PCR machine (Applied Biosystems). Data were normalized to the expression of the reference

gene *GaPDH*, which gave consistent average values in this study. Samples were run in duplicates, and relative expression was calculated using $2^{-\text{ddCt}}$ and the ddCt was calculated as $\text{dCt}[\text{goi}_{\text{SCI}} - \text{ref}_{\text{SCI}}] - \text{dCt}[\text{goi}_{\text{Sham}} - \text{ref}_{\text{Sham}}]$, where *goi* are the genes of interest and *ref* is the reference gene. For descriptive and statistical analyses, ddCt was applied as continuous variable. The mean for each gene of interest for the sham group was calculated and used to normalize the other groups in order to provide indication as to how expression levels are regulated by SCI and fracture.

Histology and histomorphometry: osteoclast activity and collagen quantification

Six femurs and tibias from each group were randomly selected for histological analysis. The entire fractured femurs and intact tibias with some adherent soft tissue were fixed in cold 4% paraformaldehyde, decalcified in cold 10% EDTA, embedded in paraffin, sectioned at 5 μm , and placed on charged slides (Manco Inc., USA). Coronal sections were stained with hematoxylin and eosin (HE) and analyzed under bright field microscopy (Axiovert; Carl Zeiss, Germany). Images were captured with a CCD camera (AxioCam MRc; Carl Zeiss, Germany) with magnifications of $\times 50$.

Adjacent sections were stained with Masson's trichrome, picosirius red, and tetrad-resistant-acid phosphatase (TRAP). Picosirius-stained sections were analyzed under polarized light microscopy AxioImager Z2 (Zeiss, Germany). Masson's and TRAP-stained sections were analyzed under bright field microscopy (Axiovert; Carl Zeiss, Germany). Images were captured with a digital camera (Zeiss). Masson's trichrome staining was used to measure the trabecular area by using the Axiovision software (ZeissTM), which identifies and quantifies trabecular bone based on the color (Supplementary Fig. 1). Quantitative results of trabecular bone were expressed as a percentage of the total metaphyseal area (%) and imaged with a magnification of $\times 50$. Picosirius red staining was used to calculate the area of collagen deposition, expressed as a percentage of the total callus area (%), with a magnification of $\times 50$. TRAP staining was used to calculate the number of osteoclasts, with a magnification of $\times 100$. Osteoclasts were counted as TRAP-positive multinucleated cells and the total number was expressed per mm^2 area of trabecular bone at the tibial metaphysis. The TRAP-positive area was measured as a percentage of the entire callus area at the fractured femur (%).

Immunohistochemistry

The expressions of osteoprotegerin (OPG), receptor activator of nuclear factor kappa-B (RANK), and the receptor activator of the nuclear factor kappa-B ligand (RANKL) were

calculated to assess bone metabolism. The sections were deparaffinized with xylene and rehydrated in graded ethanol. Antigen retrieval was performed by immersing the slides in citrate buffer and heating. Endogenous peroxidase was then blocked by immersing the slides in a 3% hydrogen peroxide solution. Immersing the slides in a 1% bovine serum albumin/PBS solution blocked unspecific ligations. Then, the slides were incubated overnight at 4 °C, with the following primary antibodies diluted in 1% bovine serum albumin: anti-RANK (Santa Cruz Biotechnology Inc., Texas, USA), anti-RANKL, anti-OPG, and either rabbit or goat IgG from control section (Vector Laboratories, Burlingame, CA, USA), depending on the primary antibody. Sections were washed and incubated in biotinylated secondary antibody (goat antirabbit and rabbit antigoat). Then, sections were washed and incubated with the avidin-biotin-peroxidase complex (ABC Kit, Vector labs) to amplify the target antigen signal. The slides were rewashed, incubated in 3,3' diaminobenzidine solution (DAB; Sigma-Aldrich Corp), and counterstained with Harris' hematoxylin. Images were captured using light microscopy, AxioImager Z2 (Zeiss, Germany) at a magnification of $\times 100$. OPG, RANK, and RANKL-positive areas were measured as a percentage of the total area.

Bone densitometry and X-Ray microtomography (μCT)

Bone densitometry analysis was performed on the fractured femurs and the intact tibias ($n = 6/\text{bone}/\text{group}$) by Dual-energy X-ray absorptiometry (DXA) using a Lunar DPX-IQ densitometer (Lunar; software version 4.7e, GE Healthcare, United Kingdom). A 90 mm^2 region of interest was used to assess the tibial proximal metaphysis. Bone mineral density (BMD, g/cm^2) and bone mineral content (BMC, g) were measured. For femurs, the entire callus was selected to assess BMD, BMC, and area (region of interest, cm^2). The scanning reproducibility (4%) was assessed by the root mean square coefficient of variation. After DXA assessment, bones were scanned using a μCT device (SkyScan 1272v2; Bruker-microCT, Belgium) at 100 kV using a 0.11-mm-thick copper filter to optimize the contrast, a 360° rotation step of 0.45°, two-frame averaging, and an isotropic resolution of 16.2 μm . Images of each specimen were reconstructed with specific software (NRecon v.1.6.3). Bones were analyzed using CT scan software (CTAn v.1.15.4) to determine morphometric parameters in selected regions of interest (ROI). All morphometric parameters are in accordance with ASBMR nomenclature.

Trabecular microstructure assessment

The trabecular bone was assessed in the proximal metaphyseal region of the nonfractured tibias, starting

immediately distal to the proximal growth plate for an extent of 3 mm. The following morphometric parameters were measured: bone volume (BV, mm³), bone volume fraction (BV/TV, %), trabecular number (Tb.N, 1/mm), trabecular thickness (Tb.Th, mm), trabecular separation (Tb.Sp, mm), density of connectivity (Conn.D, 1/mm³), tissue mineral density (TMD, g/cm³), and bone surface (BS/BV, mm).

Cortical microstructure assessment

The cortical bone was assessed in the diaphyseal region of nonfractured tibias, starting 8 mm distal to the proximal growth plate for an extent of 2 mm. Cortical volume (Ct.V, mm³), cortical volume fraction (Ct.BV/TV, %), the average cortical thickness (Ct.Th, mm), and tissue mineral density (TMD, g/cm³) were measured.

Bone callus microstructure assessment

The entire bone callus was selected to measure the callus volume (Ca.V, mm³), the woven bone fraction, which was expressed as a percentage of the callus volume and interpreted as the callus mineralization (Ca.BV/TV, %), callus porosity (Ca.Po, %), tissue mineral density (TMD, g/mm³), density of connectivity (Conn.D, 1/mm³), and the newly formed trabecular thickness (Tb.Th, mm), separation (Tb.Sp, mm), and number (Tb.N, 1/mm).

Biomechanical test

After DXA and μ CT nondestructive assessments, the nonfractured tibias were mechanically examined by a three-point-bending test, and the fractured femurs were tested in torsion. A universal testing machine was used for the tibial bending test, with a 200 N load cell (EMIC, PR, Brazil). The bone was placed on two metallic supports, 14.0 mm apart, and the load was vertically applied at the diaphysis, using a constant displacement rate of 2.0 mm/min. The load-deflection curve was obtained in real time, and the maximal load and stiffness were calculated (TESC software). The fractured femurs were placed in a custom torsion testing machine with a 2.0 Nm load cell (Instron 55MT) and tested in anticlockwise rotation at 0.5 °/s, until failure. Using the specific software script, raw data were filtered and maximum torque, stiffness, and angular displacement at failure were measured. Bones were kept wet with saline during the test.

Statistical analysis

Our primary outcome parameter for the sample size calculation was the maximal load obtained from a previous study

[12], which we have considered the difference between means from the groups Sham and SCI and the standard deviation. By using a two-sample *t*-test, our calculation indicated that at least four rats per group were sufficient to obtain a 90% power for detecting the difference between means and $\alpha = 0.05$. Therefore, we chose for a final sample size of six rats in each group. Continuous variables were expressed as means and standard deviations (SD). The results were compared using a *t*-test, where *p* values less than 0.05 were considered statistically significant. In order to control the Type I error rate from multiple comparisons, we have used the Benjamini–Hochberg False Discovery Rate (FDR, Supplementary Table 1). All statistical analyses were performed with RStudio 1.0.153 (RStudio, Inc., USA).

Results

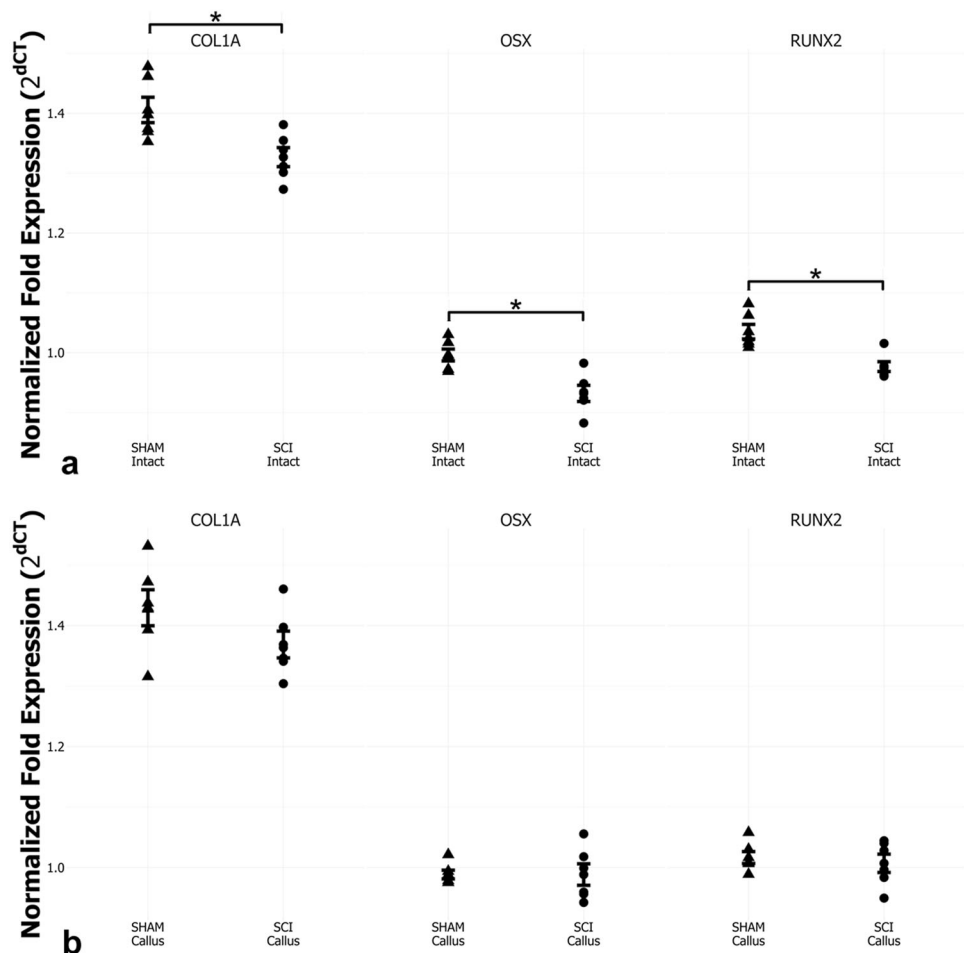
Postoperative complications were common in SCI rats, as previously described [17]. The addition of femoral fractures to these animals increased the mortality rate. Our attrition rate corresponded to 41% due to SCI (i.e., bladder rupture, autophagia, anesthetic induction, renal infection, ascites, respiratory failure, and intestinal dysfunctions), and 10% due to bone fracture intervention in animals with paraplegia (i.e., anesthesia, excessive comminution of fracture, and wire loosening). Therefore, our results are based on a sample size of 18 rats for each group.

At the beginning of the experiment, there was no significant difference in the body mass ($p = 0.3$) between the groups: 207 ± 15 g for sham versus 211 ± 15 g for SCI. On day 10, a significant difference was observed between the age-matched sham-operated rats and the animals with paraplegia: 293 ± 20 g for sham versus 238 ± 20 g for SCI, with a mean (95% CI) between-group difference of 55 g (43.79 to 66.21) and $p < 0.00001$, where the SCI group failed in gaining body mass compared with the sham group (13% versus 42%). On day 24 post-SCI, the body mass of the SCI group remained lower than controls: 402 ± 40 g for sham versus 299 ± 35 g for SCI, with a mean (95% CI) between-group difference of 104 g (85.96 to 121.26), $p < 0.00001$ and, as a result, so did the overall gain in body mass (42% versus 99%).

SCI decreased the expression of osteoblastic-related genes in the nonfractured bones

Compared with controls, SCI significantly downregulated the expression of osteoblastic-related genes, with a mean (95% CI) between-group difference of 0.08 (0.04–0.12) and $p = 0.01$ for *Col1 α 1*; 0.10 (0.05 to 0.14) and $p = 0.004$ for *Osx*; and 0.08 (0.05 to 0.11) and $p = 0.003$ for *Runx2*,

Fig. 1 **a** SCI decreased the expression of osteoblast-related genes at several stages of osteoblast differentiation. Values were normalized to GaPDH expression. Bars indicate standard error and asterisks indicate significant difference ($p < 0.05$). **b** SCI did not decrease the expression of osteoblast-related genes in the fracture callus. Values were normalized to GaPDH expression. In order to plot all genes of interest in the same graph, the dCT was log transformed. Bars indicate standard error



impairing bone formation at several stages of osteoblast differentiation (Fig. 1a).

SCI increased resorption activity, thus reducing trabecular area

Histomorphometric and immunohistochemical analyses revealed an expressive and significant increase in the resorption activity in SCI rats. The TRAP staining sections (Fig. 2a) evidenced a significant twofold increase in the number of osteoclasts per trabecular area in the SCI group when compared with controls ($0.98 \pm 0.11/\text{mm}^2$ versus $0.51 \pm 0.07/\text{mm}^2$, Fig. 2b), with a mean (95% CI) between-group difference of $0.465/\text{mm}^2$ (0.36–0.57) and $p = 0.00001$. In order to provide evidence for staining specificity, the Fig. 2c represents the negative control, in which the primary antibody was omitted and the absence of staining is a control for nonspecific binding of the secondary antibody. Therefore, the stained regions in our Fig. 2d indicate specific antibody binding sites. The SCI group showed a significant 273% increase in the RANK-positive area ($2.35 \pm 0.20\%$ versus $0.63 \pm 0.14\%$, respectively, with a mean (95% CI) between-

group difference of 1.72% (1.54–1.90), $p < 0.00001$) and 112% in the RANKL-positive area, when compared with controls ($1.95 \pm 0.42\%$ versus $0.92 \pm 0.94\%$, respectively, with a mean (95% CI) between-group difference of 1.03% (0.72–1.35), $p = 0.001$). Although significant difference was not found between the groups, OPG-positive area was 16% lower in the SCI group, when compared with the control ($2.17 \pm 0.36\%$ versus $2.59 \pm 0.59\%$, respectively, $p = 0.37$) (Fig. 2d). In addition, we detected a marked 54% reduction in the trabecular area in the SCI group when compared with controls ($6.85 \pm 2.41\%$ versus $14.87 \pm 2.47\%$, with a mean [95% CI] between-group difference of 8.02% [5.83–10.22], $p = 0.0002$, Fig. 2e, f).

SCI significantly decreased bone density, associated with trabecular and cortical microarchitecture deterioration, thus leading to weaker bones

Bone mineral density (BMD) and bone mineral content (BMC) were significantly lower in the SCI group when compared with sham rats (43% and 70%, respectively, with a mean (95% CI) between-group difference of 0.034 g/cm^2

Fig. 2 **a** Arrows indicate TRAP-positive cells and represent the number of mature osteoclasts. **b** The SCI group had twofold more TRAP-positive cells per area of trabecular bone at the proximal tibial metaphysis than controls. **c** Negative control image confirming the staining specificity in Fig. 2d. The primary antibody was omitted and the absence of staining is a control for nonspecific binding of the secondary antibody. Arrowheads indicate positive immunostained cells. **d** Immunohistochemistry demonstrates a significant increase in the expression of RANK and RANKL in the SCI group, when compared with controls. Arrowheads indicate positive immunostained cells. **e** Histological sections stained with HE show a marked loss of trabecular bone in the SCI group. **f** The SCI rats showed a significant 54% decrease in the trabecular area when compared with controls. Bars indicate standard error and asterisks indicate significant difference ($p < 0.05$)

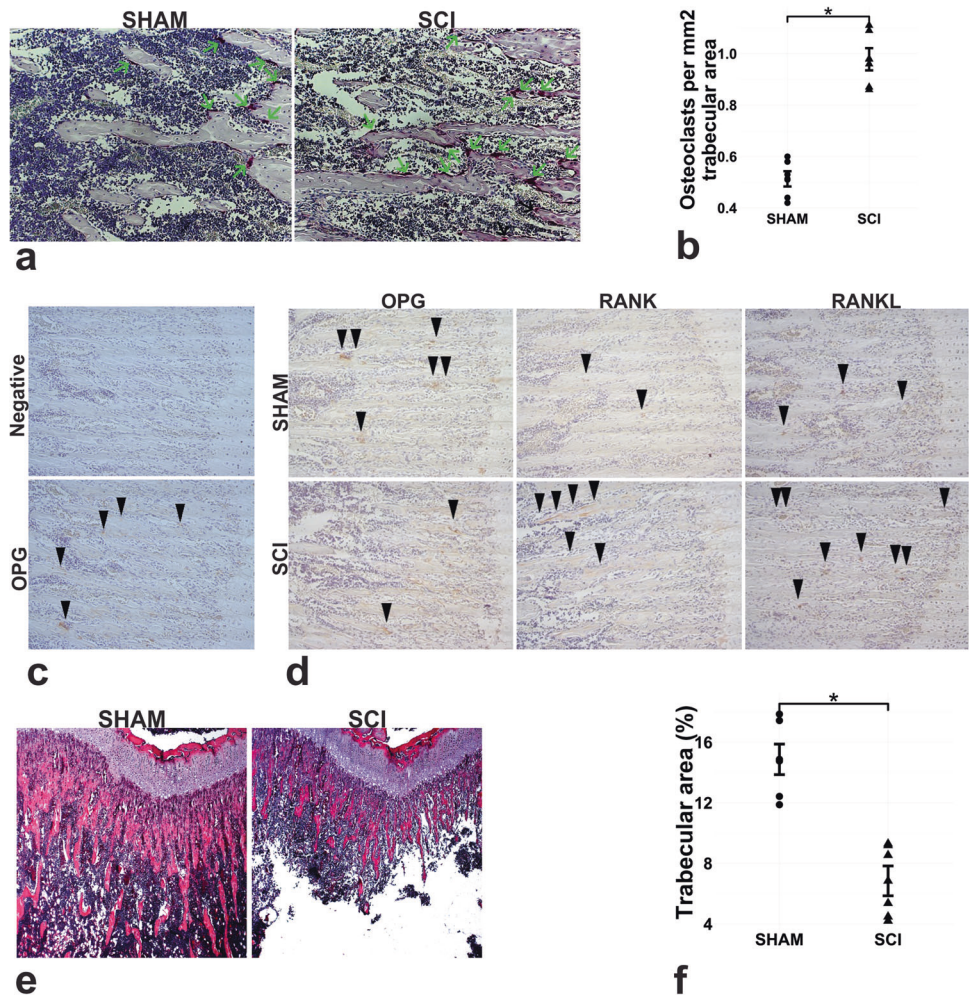


Table 1 Assessment of bone density at the proximal tibial metaphysis by DXA, and the analysis of bone microarchitecture at the metaphysis (trabecular bone) and tibial shaft (cortical bone) by μ CT. Values are means \pm standard deviation, $n = 6$ /group

	Sham	SCI	Difference mean (95% CI)	<i>p</i> value
DXA				
BMD (g/cm ²)	0.07 \pm 0.01	0.04 \pm 0.008 ^a	0.03 (0.03–0.04)	0.0005
BMC (g)	0.006 \pm 0.001	0.003 \pm 0.001 ^a	0.003 (0.002–0.004)	0.0006
μCT at trabecular bone				
BV (mm ³)	3.19 \pm 1.86	0.70 \pm 0.40 ^a	2.48 (1.38–3.59)	0.02
BV/TV (%)	6.68 \pm 4.57	1.81 \pm 1.02 ^a	4.88 (1.93–7.82)	0.05
Tb.Th (mm)	0.05 \pm 0.004	0.04 \pm 0.004 ^b	0.005 (0.002–0.008)	0.07
Tb.N (mm)	1.22 \pm 0.86	0.39 \pm 0.23 ^b	0.83 (0.33–1.32)	0.07
Tb.Sp (mm)	0.61 \pm 0.34	1.10 \pm 0.21 ^a	0.50 (0.23–0.76)	0.01
TMD (g/cm ³)	0.30 \pm 0.05	0.27 \pm 0.01 ^a	0.03 (0.01–0.04)	0.2
Conn.D (1/mm)	74.61 \pm 68.75	23.85 \pm 8.19	50.75 (5.85–95.66)	0.1
BS/BV (mm)	86.97 \pm 3.40	94.81 \pm 10.46	7.85 (2.55–13.14)	0.1
μCT at cortical bone				
Ct.V	7.51 \pm 0.67	5.01 \pm 0.52 ^a	2.49 (2.03–2.96)	0.00004
Ct.BV/TV (%)	70.03 \pm 2.97	58.39 \pm 5.97 ^a	11.64 (15.44–7.83)	0.003
Ct.Th (mm)	0.25 \pm 0.05	0.22 \pm 0.03	0.035 (0.005–0.07)	0.2
TMD (g/cm ³)	0.35 \pm 0.03	0.32 \pm 0.01 ^b	0.03 (0.01–0.05)	0.08

^a $p < 0.05$ versus Sham

^b $p < 0.08$ versus Sham

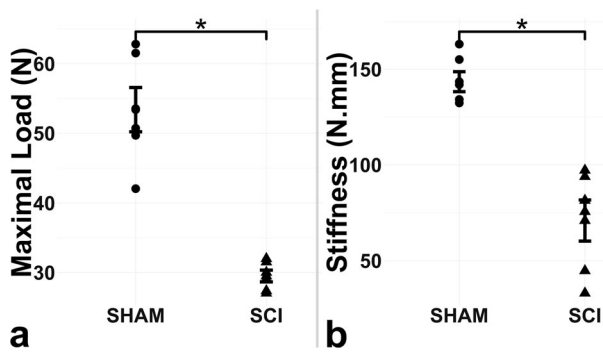


Fig. 3 SCI significantly impaired the mechanical strength, both the maximal load (**a**) and stiffness (**b**), of nonfractured bone in comparison with Sham. Bars indicate standard error and asterisks indicate significant difference ($p < 0.05$)

(0.03–0.04), $p = 0.0005$ for BMD and 0.003 g (0.002–0.004), $p = 0.0006$ for BMC, Table 1). The μ CT assessment evidenced that SCI resulted in substantial loss of both trabecular and cortical bone tissue, with significant changes in several microstructural parameters (Table 1). In the trabecular bone, SCI decreased BV by 78% (with a mean [95% CI] between-group difference of 2.48 mm³ [1.38–3.59], $p = 0.02$), BV/TV by 73% (4.88% [1.93–7.82], $p = 0.05$), Tb.Th by 20% (0.005 mm [0.002–0.008], $p = 0.07$), Tb.N by 68% (0.83/mm [0.34–1.32], $p = 0.07$), and increased Tb.Sp by 83% (0.50 mm [0.23–0.76], $p = 0.01$) when compared with controls. At the cortical bone, SCI significantly decreased Ct.V by 33% (2.49 mm³ [2.03–2.96], $p = 0.00004$), Ct.BV/TV by 17% (11.64% [7.84–15.44], $p = 0.003$), and TMD by 9% (0.03 g/cm³ [0.01–0.05], $p = 0.08$) when compared with controls (Table 1). Supplementary Fig. 2 shows reconstructed images of trabecular and cortical bones evidencing an important bone loss following SCI.

Our mechanical test evidenced that SCI rats exhibited significantly weaker bones compared with Sham, whence the maximal load was decreased by 55% (with a mean (95% CI) between-group difference of 23.90 N [20.01–27.79], $p = 0.0004$) and the stiffness by 50% (72.49 N.mm [58.93–86.06], $p = 0.0005$) (Fig. 3).

SCI did not decrease the expression of osteoblastic-related genes at the fracture callus

Although osteoblastic-related gene expression was severely downregulated by SCI at the nonfractured bone (Fig. 1a), we did not detect any changes at the fracture callus in SCI rats compared with control animals ($p = 0.1$ for *Col1a1*, $p = 1.0$ for *Osx*, and $p = 0.6$ for *Runx2*, Fig. 1b). Furthermore, we also did not detect changes when comparing the fractured bones to the nonfractured bones for both the SCI ($p = 0.5$ for *Col1a1*, $p = 0.6$ for *Osx*, and $p = 0.3$ for *Runx2*) and

sham rats ($p = 0.3$ for *Col1a1*, $p = 0.7$ for *Osx*, and $p = 0.2$ for *Runx2*).

Changes in the bone callus microenvironment, density, and microstructure following SCI

Our histological, histomorphometric, and immunohistochemical analysis from six fractured femurs of each group revealed changes in callus formation between the rats with paraplegia and their controls. At 14 days postfracture, an abundant presence of cartilaginous tissue in the control rats was detected, but only slight cartilage formation was observed in the SCI group. In contrast, SCI rats exhibited calluses with more woven bone and trabeculae than controls. Bony bridges were undetected, and fracture gaps were observed in both groups (Fig. 4a). We detected a significant 131% increase in total collagen deposition at the callus of SCI rats when compared with controls (with a mean (95% CI) between-group difference of 6.12% (3.97–8.27), $p = 0.006$, Fig. 4b). No changes were observed in the TRAP-positive area calluses between the groups ($p = 0.9$, Fig. 4c). The Fig. 4d represents the negative control confirming that the stained regions in our Fig. 5e indicate specific antibody binding sites. Our immunohistochemical analysis revealed that the SCI group showed a significant 75% ($p = 0.00005$) and 52% ($p < 0.00001$) decrease in the OPG and RANKL-positive areas, with a mean (95% CI) between-group difference of 5.60% (4.58–6.62) and 1.15% (0.97–1.33), respectively (Fig. 4e). As a result, the SCI rats exhibited bone calluses with a significant 41% lower BMD (0.06 g/cm² [0.04–0.07], $p = 0.00004$) and 29% BMC (0.02 g [0.01–0.02], $p = 0.0006$), when compared with the sham rats, in spite of statistically similar areas ($p = 0.3$, Table 2). Furthermore, our μ CT assessment showed changes in bone callus microarchitecture following SCI (Table 2). Although bone calluses in the SCI rats showed a 17% increase in the trabeculae number when compared with controls (0.43 1/mm [0.13–0.74], $p = 0.08$), they were 13% thinner (0.01 mm [0.02–0.004], $p = 0.03$) and porosity was 5% higher in the animals with paraplegia (4.01% [2.14–5.88], $p = 0.007$). Supplementary Fig. 3 shows reconstructed images of bone callus evidencing microstructural changes due to SCI, in which more osseous callus formation can be seen when compared with the shams.

Reduction in calluses strength following SCI

SCI impaired bone callus mechanical integrity (Fig. 5) by reducing the maximal torque (–44%, with a mean (95% CI) between-group difference of 0.04 N.m [0.03–0.05], $p = 0.0008$), stiffness (–33%, 2.36 N.mm/deg [0.87–3.85], $p = 0.08$), and ultimate angle (–62%, 27.53 deg [14.13–40.94], $p = 0.004$). Maximal torque corresponds to the highest load

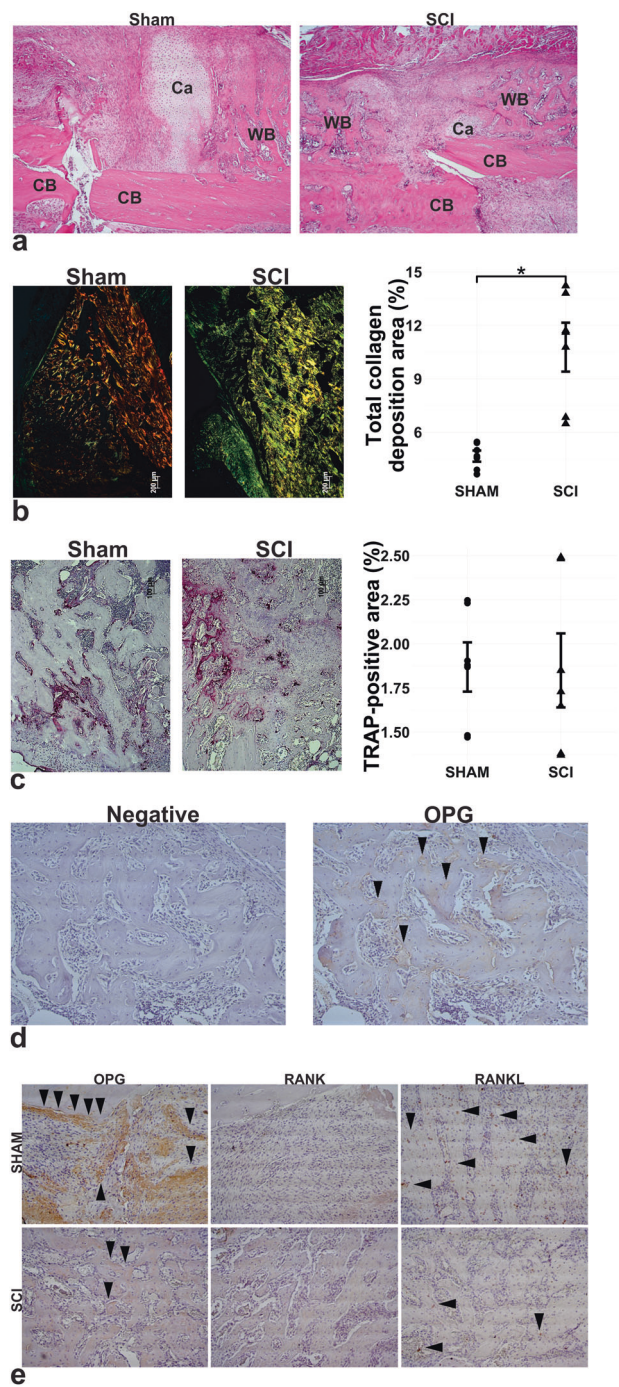


Fig. 4 **a** HE-stained histological images of the fracture evidencing an immature callus with abundant cartilaginous tissue, woven bone, and few trabeculae in the bone callus of healthy rats (Sham). SCI rats exhibited slight cartilaginous tissue and more presence of woven bone and trabeculae than the control rats. Magnification of $\times 25$. **b** Picosirius-stained slides evidencing the deposition of type 3 collagen (represented by green channel) and type 1 collagen (red channel). The histomorphometric analysis showed more (total) collagen deposition in the SCI group when compared with the controls. Magnification of $\times 50$. **c** TRAP-stained slides and histomorphometric analysis revealed no changes between groups with regards to the number of osteoclasts. Magnification of $\times 100$. **d** Negative control images to confirm the staining specificity in **e**. The primary antibody was omitted and the absence of staining is a control for nonspecific binding of the secondary antibody. Arrowheads indicate positive immunostained cells. **e** Immunohistochemistry evidencing a significant decrease in the expression of OPG and RANKL in the SCI group when compared with the controls. Arrowheads indicate positive immunostained cells. Magnification of $\times 100$. Bars indicate standard error and asterisks indicate significant difference ($p < 0.05$). CB cortical bone, Ca cartilage tissue, WB woven bone tissue

Discussion

In this study, we report that SCI significantly decreases bone mass. This finding is associated with markedly reduced bone formation and increased osteoclast activity, which resulted in disruption of bone microarchitecture and strength in a rodent model of complete SCI. Furthermore, we revealed changes in bone healing following SCI, leading to a disruption in cell differentiation and maturation and resulting in deficient callus formation.

Although the pathophysiology of SCI-induced bone loss is not fully understood, we know that an injury at the spinal cord results in changes in several organs and systems, involving several pathways in the mechanism of sublesional bone loss following neurological damage. Previous clinical studies analyzed bone turnover markers in SCI individuals and concluded that bone loss in SCI was caused by increased bone resorption, with no changes in bone formation [18]. Our TRAP histological stained sections and immunomarkers evidenced a significant increase in the osteoclastic activity in the SCI rats, as also demonstrated by Morse et al. These authors also noted a loss of normal cellular organization at the growth plate and speculated an altered cartilage differentiation and/or signaling between cartilage and bone following SCI [19]. We additionally evidenced a significant reduction in the expression of osteoblastic-related genes at different stages of osteoblast maturation following SCI.

Therefore, we have shown that SCI induces a simultaneous overactivity of osteoclasts associated with decreased osteoblastic activity, thus resulting in severe bone loss following injury. Previous authors also noted similar results, where they found a highly uncoupled bone turnover due to SCI [19–21]. Otzel et al. characterized the time courses of

prior to failure and the ultimate angle represents the deformation when the fracture occurs. A bone that tolerates higher ultimate angle is considered stronger as it can absorb more energy and present higher deformation before fracturing. Resilience is the ability of a material to absorb energy when it is deformed elastically, and release that energy upon unloading. Therefore, bone healing following SCI resulted in calluses with lower strength and resilience (despite the increased collagen deposition) when compared with the age-matched healthy animals.

Fig. 5 SCI significantly impaired the mechanical strength of fracture calluses. **a** Torque; **b** stiffness; **c** angle. Bars indicate standard error and asterisks indicate significant difference ($p < 0.05$)

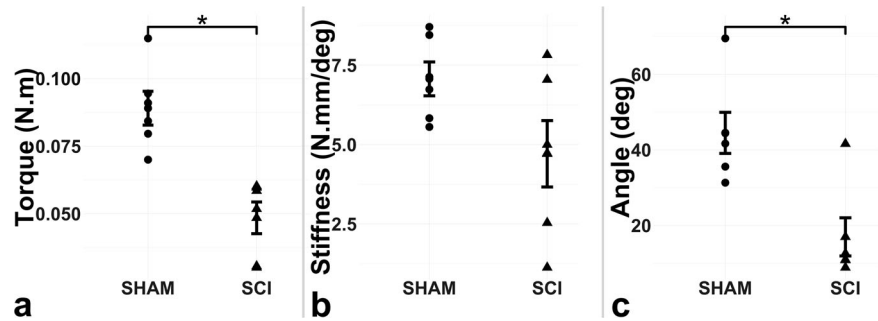


Table 2 Assessment of callus density by DXA and callus microarchitecture by μ CT. Values are means \pm standard deviation, $n = 6$ /group

	Sham	SCI	Difference mean (95% CI)	<i>p</i> value
DXA data				
BMD (g/cm^2)	0.17 ± 0.009	0.11 ± 0.02^a	0.06 (0.04–0.07)	0.00004
BMC (g)	0.07 ± 0.01	0.05 ± 0.007^a	0.02 (0.01–0.02)	0.01
Area (cm^2)	0.40 ± 0.07	0.45 ± 0.07	0.05 (0.01–0.1)	0.3
μ CT callus				
Ca.V (mm^3)	30.34 ± 7.56	25.38 ± 5.79	4.95 (0.73–9.18)	0.2
Ca.BV/TV (%)	22.82 ± 2.81	24.06 ± 5.16	1.24 (2.36–4.84)	0.6
Th (mm)	0.08 ± 0.009	0.07 ± 0.005^a	0.01 (0.004–0.02)	0.03
N (1/mm)	2.55 ± 0.45	2.98 ± 0.30^b	0.43 (0.13–0.74)	0.08
Sp (mm)	0.25 ± 0.04	0.26 ± 0.05	0.02 (0.02–0.06)	0.5
TMD (g/cm^3)	0.06 ± 0.04	0.08 ± 0.06	0.03 (0.02–0.07)	0.4
Conn.D (1/ mm^3)	285.75 ± 38.70	274.90 ± 23.29	10.85 (12.32–34.03)	0.6
Ca.Po (%)	76.07 ± 1.86	80.08 ± 2.18^a	4.01 (2.14–5.88)	0.007

^a $p < 0.05$ versus Sham

^b $p = 0.08$ versus Sham

trabecular and cortical bone losses in rats with SCI and evidenced an acute uncoupled bone turnover at two weeks postinjury, leading to significant impairments in bone cells activity, microstructure, and strength [22]. As a result, we observed a loss in trabecular and cortical volume with a concomitant increase in the trabecular separation rate in our tridimensional microstructural data. A previous study detected cortical thinning in the SCI population by using peripheral quantitative computed tomography [23], which is highly linked to bone weakening. In fact, our mechanical tests revealed a significant loss in mechanical strength following SCI, which we attributed to both trabecular and cortical deficits. In agreement, it has been previously demonstrated a site-specific loss of bone mechanical strength following SCI, in which lower force at the distal femur was linked to trabecular loss and lower strength at the mid femur was associated with cortical loss [22].

These changes potentially increase the risk for low-impact fractures in the sublesional bones in the SCI population [24]. Statistics data suggest that 70% of SCI individuals will fracture a bone located below the injury at some point in their life [3], thus highlighting the social and medical importance of this finding. Furthermore, the

profound SCI-mediated disruption of the bone micro-environment may also lead to changes during fracture healing. However, literature is controversial regarding the effects of SCI on bone healing. While some authors have shown delayed bone healing in individuals with SCI [6, 8, 9, 23] and animals [9, 14, 15], others have shown accelerated fracture healing in both clinical [4, 10, 11] and animal studies [12, 13, 24].

To our knowledge, eight animal studies have investigated the changes in fracture healing due to SCI, but none of them has fully elucidated how bone heals after the injury. Furthermore, the experimental design set in each of these studies differ from each other, making comparisons and conclusions difficult to be drawn. Three investigations evidenced a delay in bone healing when bone was fractured at two [14, 15] or three weeks post-SCI [25]. Nevertheless, Medalha et al. adopted the model of cylindrical defect, which heals differently than the bicortical fracture and does not mimic clinical conditions in patients with SCI, and the other two studies did not investigate the mechanisms leading to a delayed bone healing in SCI rats. Three other studies, in whose fractures were performed at the same time as the neurological injury, detected enhanced bone healing

due to SCI [12, 13, 26]. However, Sakitani et al. performed bilateral bicortical fracture in femurs, which may compromise bone healing in the weight-bearing control rats. Therefore, it could have led the authors to conclude that SCI accelerates healing in paraplegic rats when in fact, the real change occurred within the control group. Furthermore, clinical outcomes of disrupted bone healing in SCI people occur when bones are fractured in the onset of bone loss due to the paralysis. In fact, Miyamoto et al. detected earlier bone union in SCI rats than in controls when bone was fractured at the same time as the injury [27]. Conversely, these authors reported delayed healing with longer intervals between SCI and bone fracture, but this study lacked in elucidating the mechanisms and callus characterization. Furthermore, Aro et al. observed that in spite of healing faster, the calluses formed in SCI rats when bones were fractured at the same time of injury displayed incomplete maturation of woven bone [28]. Taking all these into consideration and in order to better mimic clinical conditions in where people with SCI sustain an additional bone fracture, we opted to induce bone fracture ten days after the neural injury, in which bone loss has already been established [19].

In this study, we evidenced several changes in bone healing due to SCI and fracture. The histological analysis revealed that SCI rats exhibited calluses with more trabeculae and collagen deposition than the controls. Curiously and in spite of the tremendous downregulation of the osteoblastic-related gene expression due to the SCI at the nonfractured bones, we did not detect any changes at the fracture callus, which seems to be linked to our histological evidences of accelerated bone healing in SCI. We attributed the accelerated bone formation to the mostly intramembranous ossification that occurred in SCI animals at 14 days postfracture. In control rats, the bone healing at the same time-point occurred mainly by endochondral ossification analysis, with an abundant presence of cartilaginous tissue at the callus. Sakitani et al. [12] followed bone healing in SCI rats and also found that early bone fracture healing in rats with paraplegia occurred mostly through intramembranous ossification, in contrast with the endochondral ossification displayed by the controls. Endochondral ossification involves the formation of intermediate cartilaginous tissue with subsequent remodeling into bone tissue, which requires more time. The authors showed that despite healing faster, the callus of SCI rats was weaker than the calluses of the controls. In our study, we also evidenced by a mechanical torsion test and showed lesser mechanical integrity. Furthermore, we revealed that SCI resulted in calluses with lower flexibility, despite showing more collagen deposition than the controls. We believe that SCI induced a defect in the trabecular structure quality and collagen production, which may be linked to our immunohistochemical data evidencing a marked decrease in OPG

expression in rats with paraplegia. Furthermore, we demonstrated by DXA that these calluses were less dense (BMD and BMC) than the controls, which was also found in the study of Ding et al. [14]. We also examined the microarchitecture of the calluses by μ CT and demonstrated that although there were more trabeculae in the SCI rats, they were thinner and callus is more porous, highlighting the lesser quality of these calluses despite the early trabecular formation.

Therefore, the changes in the mechanism of bone healing in SCI rats led to the formation of calluses with more early trabeculae, despite being thinner and less dense. Although the collagen deposition has shown to be higher in the SCI rats, the lower expression of OPG in the callus may lead to disruption in the trabecula maturation and integrity, leading to weaker and less flexible callus. It is important to highlight that we have used the Benjamini–Hochberg False Discovery Rate in order to control the type I error rate due to the multiple statistical comparisons conducted in this study. We inform that only one variable (trabeculae thickness at the callus) was not considered statistical significant after the adjustment of its p value. However, our tridimensional microcomputed images associated with our histological findings encourage us to state that the calluses in the SCI rats are formed by thinner trabeculae than the shams. Furthermore, the p value for this variable (0.03) remained lower than its FDR (0.3). Therefore, we opted to use the p value in our figures, graphs, tables, and throughout this manuscript.

Limitations of this study include only one time-point analysis following bone fracture. However, our previous experience in bone healing in rodents and related publications support our study design at choosing the most likely crucial period for callus formation in rats with paraplegia. Another limitation of this study refers to the use of seven-week-old male rats, which are equivalent to adolescent human who are not the majority of people with SCI. However, using musculoskeletal maturity to determine adulthood in rats is difficult because unlike humans, the growth plates of long bones remain open in rats permitting skeletal growth until 32 to 36 weeks [29]. Furthermore, to our knowledge, all publications investigating the effects of SCI on bone quality and healing used rats within skeletal growth, even when they were considered adults by the authors [30]. In most of these studies the rats aged 6–8 weeks at the time of SCI [13, 20, 25], while in others the rats were 16–18 weeks old [12, 22, 30]. Our decision and experimental refinement contributed to reduce the number of animals by minimizing unnecessary animal groups (the 3Rs). Future studies should address more mechanistic studies examining the interactions of SCI, cytokines, and bone cells during fracture healing, as well to perform these investigations in skeletally mature rats.

In conclusion, SCI induces a severe bone loss due to both increased resorption and decreased formation. SCI also leads to changes in the mechanisms of bone healing by accelerating and increasing the presence of woven bone and trabeculae at an early stage of callus formation. The calluses in the SCI rats have a worse quality than controls, with a disruption in the bone microenvironment, lower bone density, thinner newly formed trabeculae, more callus porosity, and lower mechanical strength and flexibility.

Data availability

The datasets generated during and/or analyzed during the current study are available from the corresponding author on reasonable request. All data generated or analyzed during this study are included in this published article.

Acknowledgements We would like to thank all of the investigators, staff, and trainees from the Laboratory of Bioengineering at the School of Medicine of Ribeirão Preto, University of São Paulo, who assisted in the entire study. We also would like to thank the 3B's Research Group as well as the School of Dentistry of Ribeirão Preto, University of São Paulo, who assisted in the microstructural analysis.

Funding AZ received financial funding by the São Paulo Research Foundation (FAPESP) - 2015/22126-1.

Author contributions MMB and KA performed the experiments, analyzed the findings, and contributed to the manuscript preparation. MMB, JPBX, VMC, RLR, RBS, JBV, and AZ analyzed the data and revised the manuscript. JBV and AZ composed the research proposal, conceived and designed the experiments, discussed all of the results, and wrote the manuscript. All authors revised the paper critically for intellectual content and approved the final version. All authors agree to be accountable for the work and to ensure that any questions relating to the accuracy and integrity of the paper are investigated and properly resolved.

Compliance with ethical standards

Conflict of interest The authors declare that they have no conflict of interest.

Ethical statement The Institutional Animal Care and Use Committee approved all experiments and animal care carried out in this study (protocol 199/2015). We certify that all applicable institutional and governmental regulations concerning the ethical use of animals were followed during the course of this research.

Publisher's note Springer Nature remains neutral with regard to jurisdictional claims in published maps and institutional affiliations.

References

- Morse LR, Battaglini RA, Stolzmann KL, Hallett LD, Waddimba A, Gagnon D, et al. Osteoporotic fractures and hospitalization risk in chronic spinal cord injury. *Osteoporos Int*. 2009;20:385–92.
- Sugawara H, Linsenmeyer TA, Beam H, Parsons JR. Mechanical properties of bone in a paraplegic rat model. *J Spinal Cord Med*. 1998;21:302–8.
- Szollar SM, Martin EM, Sartoris DJ, Parthemore JG, Deftos LJ. Bone mineral density and indexes of bone metabolism in spinal cord injury. *Am J Phys Med Rehabil*. 1998;77:28–35.
- Wang L, Yao X, Xiao L, Tang X, Ding H, Zhang H, et al. The effects of spinal cord injury on bone healing in patients with femoral fractures. *J Spinal Cord Med*. 2014;37:414–9.
- Schulte LM, Scully RD, Kappa JE. Management of lower extremity long-bone fractures in spinal cord injury patients. *J Am Acad Orthop Surg*. 2017;25:e204–e213.
- Gifre L, Vidal J, Carrasco JL, Muxi A, Portell E, Monegal A, et al. Risk factors for the development of osteoporosis after spinal cord injury. A 12-month follow-up study. *Osteoporos Int*. 2015;26:2273–80.
- Zamarioli A, Maranhão DA, Butezloff MM, Moura PA, Volpon JB, Shimano AC. Anatomic changes in the macroscopic morphology and microarchitecture of denervated long bone tissue after spinal cord injury in rats. *Biomed Res Int*. 2014;2014:853159.
- Grassner L, Klein B, Maier D, Bühren V, Vogel M. Lower extremity fractures in patients with spinal cord injury characteristics, outcome and risk factors for non-unions. *J Spinal Cord Med*. 2017;41:1–8.
- Wang L, Liu L, Pan Z, Zeng Y. Serum leptin, bone mineral density and the healing of long bone fractures in men with spinal cord injury. *Bosn J Basic Med Sci*. 2015;15:69–74.
- Khallaq FG, Kehinde EO, Mostafa A. Growth factors and cytokines in patients with long bone fractures and associated spinal cord injury. *J Orthop*. 2016;13:69–75.
- Ragnarsson KT, Sell GH. Lower extremity fractures after spinal cord injury: a retrospective study. *Arch Phys Med Rehabil*. 1981;62:418–23.
- Sakitani N, Iwasawa H, Nomura M, Miura Y, Kuroki H, Ozawa J, et al. Mechanical stress by spasticity accelerates fracture healing after spinal cord injury. *Calcif Tissue Int*. 2017;101:384–95.
- Wang L, Tang X, Zhang H, Yuan J, Ding H, Wei Y. Elevated leptin expression in rat model of traumatic spinal cord injury and femoral fracture. *J Spinal Cord Med*. 2011;34:501–9.
- Ding WG, Jiang SD, Zhang YH, Jiang LS, Dai LY. Bone loss and impaired fracture healing in spinal cord injured mice. *Osteoporos Int*. 2011;22:507–15.
- Ding WG, Liu JB, Wei ZX. Spinal cord injury causes more damage to fracture healing of later phase than ovariectomy in young mice. *Connect Tissue Res*. 2012;53:142–8.
- Santiago HA, Zamarioli A, Sousa Neto MD, Volpon JB. Exposure to secondhand smoke impairs fracture healing in rats. *Clin Orthop Relat Res*. 2017;475:894–902.
- Zamarioli A, Battaglini RA, Morse LR, Sudhakar S, Maranhão DA, Okubo R, et al. Standing frame and electrical stimulation therapies partially preserve bone strength in a rodent model of acute spinal cord injury. *Am J Phys Med Rehabil*. 2013;92:402–10.
- Maimoun L, Couret I, Micallef JP, Peruchon E, Mariano-Goulart D, Rossi M, et al. Use of bone biochemical markers with dual-energy X-ray absorptiometry for early determination of bone loss in persons with spinal cord injury. *Metabolism*. 2002;51:958–63.
- Morse L, Teng YD, Pham L, Newton K, Yu D, Liao WL, et al. Spinal cord injury causes rapid osteoclastic resorption and growth plate abnormalities in growing rats (SCI-induced bone loss in growing rats). *Osteoporos Int*. 2008;19:645–52.
- Jiang SD, Jiang LS, Dai LY. Effects of spinal cord injury on osteoblastogenesis, osteoclastogenesis and gene expression profiling in osteoblasts in young rats. *Osteoporos Int*. 2007;18:339–49.
- Zhao W, Li X, Peng Y, Qin Y, Pan J, Li J, et al. Sclerostin antibody reverses the severe sublesional bone loss in rats after chronic spinal cord injury. *Calcif Tissue Int*. 2018;103:443–54.
- Otzel DM, Conover CF, Ye F, Phillips EG, Bassett T, Wnek RD, et al. Longitudinal examination of bone loss in male rats after

- moderate-severe contusion spinal cord injury. *Calcif Tissue Int.* 2019;104:79–91.
23. Eser P, Schiessl H, Willnecker J. Bone loss and steady state after spinal cord injury: a cross-sectional study using pQCT. *J Musculoskelet Neuronal Interact.* 2004;4:197–8.
 24. Frotzler A, Cheikh-Sarraf B, Pourtehrani M, Krebs J, Lippuner K. Long-bone fractures in persons with spinal cord injury. *Spinal Cord.* 2015;53:701–4.
 25. Medalha CC, Santos AL, Veronez Sde O, Fernandes KR, Magri AM, Renno AC. Low level laser therapy accelerates bone healing in spinal cord injured rats. *J Photochem Photobio, B.* 2016;159: 179–85.
 26. Aro H, Eerola E, Aho AJ, Penttinen R. Healing of experimental fractures in the denervated limbs of the rat. *Clin Orthop Relat Res.* 1981;155:211–7
 27. Miyamoto T. An experimental study on fracture healing in paraplegic rats. *Nihon Seikeigeka Gakkai Zasshi.* 1987;61:1135–45.
 28. Aro H, Eerola E, Aho AJ. Fracture healing in paraplegic rats. *Acta Orthop Scand.* 1985;56:228–32.
 29. Quinn R. Comparing rat's to human's age: how old is my rat in people years? *Nutrition.* 2005;21:775–7.
 30. Lin T, Tong W, Chandra A, Hsu SY, Jia H, Zhu J, et al. A comprehensive study of long-term skeletal changes after spinal cord injury in adult rats. *Bone Res.* 2015;3:15028.